Desalination and Water Treatment
www.deswater.com

doi: 10.5004/dwt.2020.26200

203 (2020) 388–402
November

Application of a novel high-performance nano biosorbent for removal of anionic dyes from aqueous solutions using shuffled frog leaping algorithm: isotherm, kinetic and thermodynamic studies

Mahboube Shirani[a,*], Ali Akbari[a], Alireza Goli[b]

[a]*Department of Chemistry, Faculty of Science, University of Jiroft, P.O. Box: 7867161167, Jiroft, Iran, Tel. +98 3443347061; Fax: +98 34 43347065; emails: m.shirani@ujiroft.ac.ir (M. Shirani), a.akbari@ujiroft.ac.ir (A. Akbari)*
[b]*Graduate of Department of Industrial Engineering, Engineering Faculty, Yazd University, P.O. Box: 89195741, Yazd, Iran, email: alireza.g88@gmail.com (A. Goli)*

Received 11 December 2019; Accepted 5 June 2020

ABSTRACT

Curdled milk, as a novel nano biosorbent, was utilized for ultrasound-assisted removal of eosin blue and aniline blue from aqueous solutions. Curdled milk was characterized by Fourier-transform infrared spectroscopy, Brunauer–Emmett–Teller isotherm, and scanning electron microscopy-energy-dispersive X-ray spectroscopy techniques. The main factors of pH, sonication time, amount of biosorbent, temperature, and initial dye concentrations were investigated. Maximum adsorption capacities of 147.1 and 131.6 mg g^{-1} were acquired for eosin blue and aniline blue respectively at optimum conditions including pH of 3–4, biosorbent amount of 10 mg, the temperature of 25°C, time of 5 min, and initial dye concentration of 10–30 mg L^{-1}. Hybrid artificial neural network-genetic algorithm and shuffled frog leaping algorithm (SFLA) were employed for prediction and optimization of the process respectively. The results revealed that SFLA had the high capability for the optimization of the process. The biosorption data ideally fitted to the Langmuir model. Adsorption of aniline blue and eosin blue on to the curdled milk follows the pseudo-second-order kinetic model. Thermodynamic studies presented the negative values of $\Delta H°$ in which indicated the exothermic nature of the adsorption process and negative values of $\Delta G°$ showed the favorability and spontaneously occurrence of the adsorption process.

Keywords: Biosorbent; Dye removal; Anionic dye; Shuffled frog leaping algorithm

1. Introduction

Dyes are widely applied in various main industries like cloth coloring, leather treatment, printing, cosmetics, plastics, paper and pulp manufacturing, and pharmaceutical. Although dyes are considered as toxic organic pollutants, they are enormously released into the water sources [1]. Moreover, dyes remain unchanged in the aquatic system for a long time which significantly reduces the penetration of the sunlight and the oxygen as two essential factors for aquatic life. Hence, varieties of techniques such as coagulation and flocculation [2], membrane separation [3], adsorption [4], and ozonation [5] were applied to clean up dye-polluted industrial wastewater. Among them, adsorption is considerably seized attention due to its simplicity, the potential of various sorbents application, low cost, and short time process. Different synthetic sorbents such as nanoparticles [6], modified carbon nanotube [7], zeolite [8], alumina [9], and bentonite [10,11] were reported. Biosorbents are considered as green and environmentally friendly materials which intensify their importance and application [12]. Biosorbents are more preferred due to

* Corresponding author.

easy accessibility, abundance, and cheapness. Walnut shell [13], *Ageratum conyzoides* leaf powder [14], eggshell powder [15], *Chlorella pyrenoidosa* [16], sphagnum peat moss [17] are some examples of the application of non-conventional, low-cost biosorbents in dye removal processes. The ultrasound-assisted processes can efficiently applied in any extraction or removal of any contamination. In fact, the combination of ultrasonic waves with other methods can be successfully used to enhance the extraction or removal efficiencies [18]. The propagation of pressure through the solution leads to the formation, the growth and collapse of bubbles, which is called acoustic cavitation [19]. This phenomenon causes a significant enhancement of mass transfer between adsorbate and adsorbent. Therefore, the application of ultrasonic waves in the adsorption process would definitely improve the removal efficiencies of dyes from aqueous solutions. Recently, various statistical and mathematical techniques have been reported in dye removal procedures for modeling and optimization of the chemical processes to reduce the operational cost and time. Artificial neural network (ANN) is one of the most popular prediction techniques which deals with a multi-layered perceptron consisting of input, hidden layer, output, and a diverse number of neurons in each layer. Despite the significant ability of ANN in prediction, ANN is incapable of optimization because it is precisely a data-based technique. Therefore, ANN techniques were improved through the hybridization of computational intelligence techniques with neural networks called "hybrid artificial neural network" [20]. To this aim, the optimization of ANN parameters can be rectified by the genetic algorithm (GA) to obtain the best optimal conditions with the highest efficiencies. In fact, the GA optimization process is based on the weights and biases acquired by ANN. GA can be comprehensively utilized in many optimization processes with the discontinuous, stochastic, or highly nonlinear objective function. The shuffled frog leaping algorithm (SFLA) is a meta-heuristic method for efficient optimization. SFLA is based on observing, imitating, and modeling the behavior of a group of frogs that are looking for a place with the maximum amount of food [21]. SFLA basically introduced by Eusuff and Lansey [22] to solve the complicated optimization problems including nonlinear, non-differentiable, and multi-modal states. The main advantage of the SFLA is its high-speed convergence [23]. The aim of this study is to represent a novel green biosorbent in dye removal techniques. The key factor in adsorptive techniques is effective interaction between the adsorbate and the functional groups of the adsorbent. The more powerful the interactions are, the higher removal (%) obtains. Curdle milk is simply obtained from spoiled milk. Curdled milk has a polyamide structure which can efficiently interact with the target analytes and adsorb them on its surface through amide functional groups in the structure. To the best of our knowledge, this is the first report on the application of curdled milk as a biosorbent. Interestingly, according to our experiments, small amounts of curdled milk on a pen-written piece of paper can incredibly adsorb all the pen ink on the paper which intensifies the proficiency of this biosorbent comparing with other reported studies. In this study, curdled milk as a protein-based biosorbent was used for the simultaneous removal of eosin blue and aniline blue as model anionic dyes from aqueous solutions. Hybrid ANN and GA and SFLA were applied for prediction and optimization of the process.

2. Materials and method

2.1. Materials

All used chemicals in this study with the analytical grade were purchased from Merck and Sigma-Aldrich. Eosin blue (MW: 624.06 g mol^{-1}, 99%, Sigma-Aldrich, USA) and aniline blue (MW: 760.72 g mol^{-1}, ≥99.5%, Sigma-Aldrich, USA) were the anionic dyes which were removed from the aqueous solution. The standard stock solutions of eosin blue (1,000 mg L^{-1}) and aniline blue (1,000 mg L^{-1}) were obtained by dissolving the appropriate amount of dyes. Standard solutions of eosin blue and aniline blue were prepared daily using stock solutions. Ethanol (≥99.9%, Merck, Germany) was used for rinsing the biosorbent and sodium chloride (≥99.9%, Merck, Germany) was used for the determination of pH of the isoelectric point. Buffer solutions in the range of 1–9 were prepared and utilized to set the pH of the solutions. Potassium chloride (≥99.5%, Merck, Germany), hydrochloric acid (37%, Merck, Germany), acetic acid (≥99.7%, Sigma-Aldrich, USA), sodium acetate (≥99.0%, Sigma-Aldrich, USA), monopotassium phosphate (≥99.0%, Sigma-Aldrich, USA), dipotassium phosphate (≥98.0%, Sigma-Aldrich, USA), and disodium tetraborate (≥99.0%, Sigma-Aldrich, USA) were all utilized for the preparation of buffer solutions. To prepare the solutions deionized water was applied.

2.2. Instrumentation

Digital ultrasonic cleaner (CD-4820, China) was used to efficiently increase the contact surface of the biosorbent and dye molecules. Centrifuge (Selecta lab, China) was utilized to separate the biosorbent from the solution after the adsorption process. UV-visible spectrophotometer (Winlab, PerkinElmer, USA) was applied for data analysis. In order to investigate the morphological analysis of the nano biosorbent, nitrogen physisorption (at 76.09 K) by a pore size analyzer (Micromeritics ASAP 2020 V3. 04 E surface area and porosity analyzer, USA) with the adsorption-desorption isotherm at relative pressure in the range of 10^{-6}–1 was used.

2.3. Biosorbent

500 g low-fat milk (1%) was purchased from a local supermarket in Jiroft, Kerman Province, Iran. Then, it was let for 24 h at ambient temperature to become sour. the obtained sour milk was filtrated to separate the curdled part from the media. The curdled milk was rinsed with ethanol for several times to remove any possible impurities. After that, it was dried at ambient temperature for 12 h. The dried curdled milk was used for further studies.

2.4. Point of zero charges (isoelectric point) determination

In order to preserve the electrical neutrality of the water–solid interface, the surface would attain a net charge of a particular sign which completely depends on the pH, type, and amount of electrolyte solutions. The isoelectric point (pH_{IEP}) or point of zero charges (pH_{pzc}) is elucidated as the type of the surface-active centers and the adsorption ability of the surface through for linear range of pH sensitivity. The pH_{pzc} of curdled milk was investigated as follows; seven solutions containing 10 mL NaCl solution (0.01%) were prepared and the initial pH of each of these solutions was set in the range of 1–7. Then, 15 mg of the biosorbent was added to each solution and let them reach the equilibrium state for 24 h [9]. The final pH of the solutions was determined at a specific time. The pH_{PZC} was determined from initial to final pH curve, crossed by $y = x$ line on the graph which was 2.8 [24].

2.5. Ultrasonic assisted dye removal procedure

The pH of 10 mL sample solution with a concentration of 20 mg L^{-1} of eosin blue and aniline blue was adjusted to 3–4 by the relevant buffer solution. 10 mg of curdled milk was added to the solution and ultrasonicated for 5 min at room temperature. Then, the solution was transferred to a conical-bottom polypropylene tube and centrifuged for 10 min at 3,500 rpm. After that, the upper phase was separated and measured by UV-Visible spectrophotometer. As reported previously the removal percent was calculated as follows [8]:

$$\text{Removal percentage } (\%) = \frac{(C_i - C_e)}{C_i} \times 100 \quad (1)$$

In which C_i is the initial dye concentration, C_e is the equilibrium concentration or final dye concentration (the concentration of dyes in the upper phase after the adsorption process).

2.6. Modeling

2.6.1. Genetic algorithm based on a hybrid artificial neural network

ANN as a kind of artificial intelligence follows human brain behavior. ANN consists of three layers of input, hidden and output, in which the number of variables corresponds to the input neurons and the number of target output variables (output neurons). The number of hidden layers completely relies on the application of the network. GA as a potent optimization method can conquer the ANN limitations. GAs are considered as adaptive heuristic search algorithm based on the evolutionary ideas of natural selection and genetics which describe intelligent exploitation of a random search to solve the optimization problems. In fact, GAs are based on an analogy with the genetic structure and behavior of chromosomes within a population of individuals [25]. In the hidden and output layers, the net input (X_j) to node j is as follows:

$$X_j = \sum_{i=1}^{n} W_{ij} y_i + b_j \quad (2)$$

In order to obtain the hidden and output layers as transfer functions, a three-layer ANN with tan-sigmoid and purline functions were applied respectively. A sigmoid function as a bounded differentiable real function is elaborated for the real input values with a positive derivative at each point. Eq. (3) shows the tan-sigmoid transfer function [26]:

$$F(x) = \frac{1}{1 + e^{-x}} \quad (3)$$

MATLAB R2015 software was employed to create a multi-layer perceptron neural network using tan-sigmoid and purline functions as transfer functions in hidden and output layers respectively. In this research study, all the experimental data (28 data) were split into three main parts of training, validating, and testing data, in which the training data were applied. Fig. 1 shows the topology of ANN including the number of layers, neurons of each layer and they are interconnected.

When a generalized ANN model is extended, the input space would be optimized by the GA. The input vector including input parameters of the model converts the decision parameter for the GA. In fact, GA is a potent strategy for optimization which is based on the principles of natural selection. This algorithm commences with a population of random solutions in some structure series. Then, a number of operators are repeatedly used to achieve convergence. GA has the benefit of independence of the initial value. Being time-consuming is the main drawback of this technique [27]. Generally, GA development includes several steps as initialization of solution population identified as chromosomes, fitness computation based on the objective function, selection of the best chromosomes, and the genetic propagation of the chosen parent chromosomes by genetic operators like crossover and mutation. Crossover and mutation are utilized to develop the new and better populations of the chromosomes [28].

2.6.2. Shuffled frog leaping algorithm

The SFLA is a novel evolutionary algorithm that has several advantageous features including simplicity, limited parameters, quick computation, global optimization, and simple realization. In SFLA, the frog population is distributed into numerous sub-populations with diverse beliefs. Each of the sub-populations was involved in deep-searching of the confined area in the solution space using a specific approach. This is affected by the individual and combined thoughts of the frog in the sub-population evolution. Then, a fixed number of epoch's thoughts were switched in the sub-population [29]. The balanced approach between the global information interchange and the limited area deep searching assist SFLA to move toward the global optimization by jumping out the local extreme. In a target search space of D-dimensions, the random population of P frogs represents the solution, for instance, the i^{th} frog denotes the clarification of the problem $X_i = (x_{i1}, x_{i2}, ..., x_{iD})$. The arrangement of the frog population into several sub-populations (good to bad) was done based on their fitness. For example, the frog of rank 1 is allocated into the 1st sub-population, the frog of rank 2 is allocated into the 2nd sub-population, and

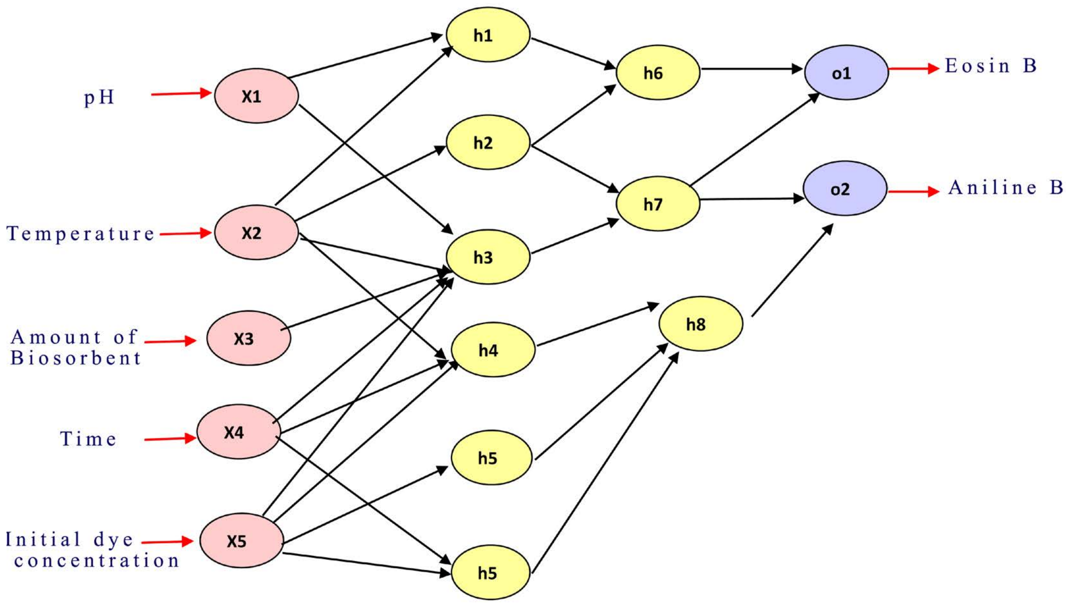

Fig. 1. The optimized topology of artificial neural networks.

the frog of rank M is allocated into the M^{th} sub-population. This process is continued till all the frogs were assigned onto some sub-population. Each of the sub-populations was employed for limited area deep-searching, which decided the poorest individual X_w, the finest one X_b, and the overall best one X_g from the sub-population in each of the iterations. The worst individual X_w was updated further. A novel X_w was produced randomly if no enhancement in the fitness value of X_w was observed, which was continued until it satisfied the update algebra condition. All frogs from different sub-population were mixed into a new sub-population after completing the local area deep-searching. Then, the local area deep searching process was continued until the decided iteration number. The pseudo-code of SFLA is demonstrated in Fig. 2.

```
Pseudo code of the shuffled frog leaping(SFL)
Begin
Randomly generate a population (p) of solution(frogs):
For each individual frog(frog);calculate fitness of i^th frog
Sort the population in descending order in their fitness;
For i=1 to number of generation;
Divide p into m memeplexes;
 For each memeplex;
Determine the best and worst frogs;
Repeat;
Improve the worst frog position using equation (1) or (2);
Until a specific number of iterations is satisfied;
End for;
End for;
Combine the evolved memeplex;
Sort the population (p) in descending order of their fitness;
Check if termination = true;
End;
```

Fig. 2. Shuffled frog leaping algorithm pseudo-code.

3. Results and discussion

3.1. Characterization of curdled milk

The structure of the novel nano biomolecule sorbent, curdled milk, was considered by scanning electron microscopy technique. Fig. 3a clearly shows the nanostructure of the curdled milk in which three sections were indicated as 34.54, 37.48, and 39.91 nm. The energy-dispersive X-ray spectroscopy (EDX) pattern of curdled milk and the chemical composition of the biosorbent containing C, N, O, P, S, and Ca is shown in Fig. 3b. N and O in the EDX pattern indicate the presence of carbohydrates and polyamide structure. P element corresponds with the casein (a family of related phosphoproteins). In order to explore the functional group of curdled milk, the Fourier-transform infrared spectroscopy (FT-IR) technique was also used. As presented in Fig. 4a the band at 3,264 cm^{-1} represents for the –NH stretching vibrations. The stretching vibrations of CH_2 and CH_3 groups of the alkyl chain exist at 2,921 and 2,853 cm^{-1}. The peak at 1,743 cm^{-1} (ν–C=O), reveals the absorption band of esters. The band peak at 1,641cm^{-1} (ν–C=O) shows the amide which confirms the amide groups in the polyamide structure of curdled milk. The bands at 1,107; 1,141; and 1,308 cm^{-1} indicate the C–O and C–N stretching. The C–O stretching at 1,234 and 1,158 cm^{-1} show the functional groups of polypeptides and amino acids. The band at 1,536 cm^{-1} (ν N–H and ν C–N) shows the amide. The C–H bending at 1,442 and 1,375 cm^{-1} represents the functional groups of polypeptides [30]. Fig. 4b represents the N_2 adsorption–desorption isotherms and pore size distributions (inset). The nitrogen sorption isotherms of curdled milk indicate representative type-IV curves with H2-type hysteresis loops in the relative pressure range between 0.4 and 1.0 which is characteristic of materials (based on the International Union of Pure and Applied Chemistry classification). Furthermore, the measured Brunauer–Emmett–Teller surface area and the average

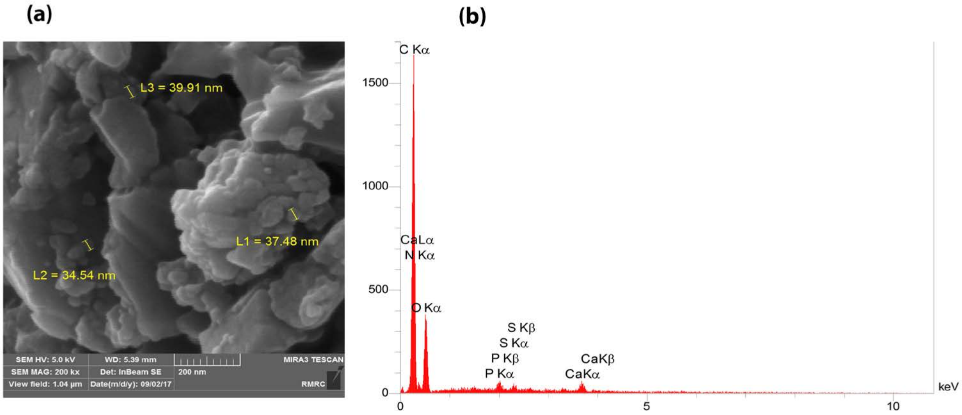

Fig. 3. Characterization analysis of curdled milk (a) the scanning electron microscopy image of the curdled milk as a nano biosorbent and (b) the EDX analysis pattern of curdled milk.

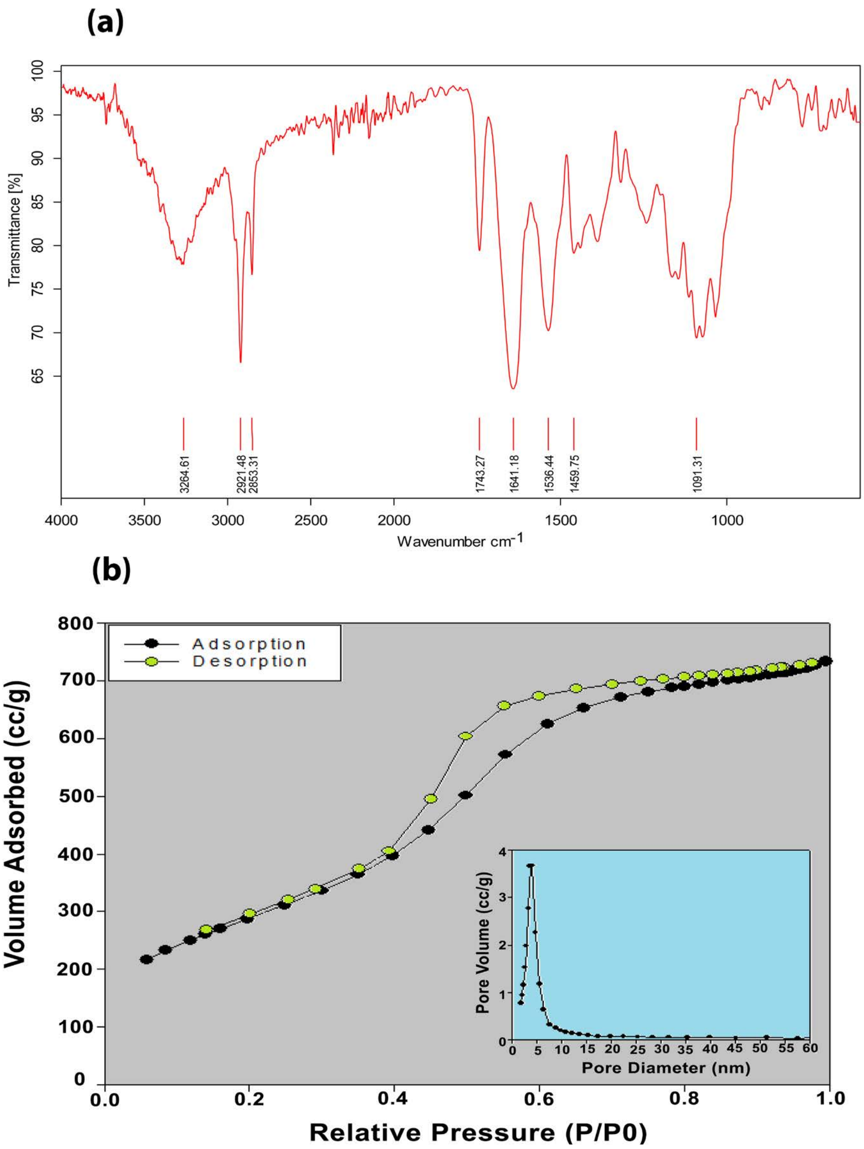

Fig. 4. Characterization analysis of curdled milk (a) the FT-IR of the curdled milk nano biosorbent and (b) nitrogen adsorption–desorption isotherms (Brunauer–Emmett–Teller results) of curdled milk.

pore size were 1,051 m^2 g^{-1} and 4.25 nm, respectively. The proper surface area, uniform pore size, and pore volume of curdled milk may provide the opportunity to adsorb the materials. High surface area and nanostructure of curdled milk result in its high adsorption capacity.

3.2. Prediction by genetic algorithm based hybrid artificial neural network

In order to evaluate the procedure of the hybrid ANN prediction; the functional values, that is, mean square error (MSE), mean absolute error (MAPE), and R^2 were used. The values of the performance criteria were checked separately for each output, that is, the dye removal (%) for eosin blue and aniline blue. ANN and the ANN combined with the GA have been implemented in the MATLAB R2015 software. The comparisons of the two methods are summarized in Table 1.

In Table 1, the value of the MSE for the traditional ANN was 0.695. But the hybrid neural network has been able to reduce the index to 0.665. The correspondence of the results of the neural network with laboratory data is above 80%, which proves the effectiveness of artificial intelligence tools in laboratory predictions. The comparison of the traditional neural network with the hybrid ANN confirms that a hybrid neural network has increased the rate of matching of the predictive data with experimental data. In other words, GA is intended to improve compliance with the experimental results by up to 10 percent. This issue can be reviewed based on the R^2 index. The relationship between the experimental data vs. predictive values based on the combined neural network showed the R^2 index of 0.9226 and 0.917 for eosin blue and aniline blue respectively which indicate the ideality of the applied model. Moreover, ANN is able to achieve the highest possible compliance with the experimental results. Accordingly, the predicted error for both eosin blue and aniline blue is very low. In other words, the error value is close to each observation. As the neural networks find the relations between the input parameters and outputs using training sets, the best matching inputs and outputs in the test set is important. The mural network should have the ability to expand the relationship in the train set to the test set. To this aim, the relative error rate (MAPE) of the traditional neural network and the combined neural network with GA were calculated for both analytes. The applied ANN and ANN-GA for both analytes had low MAPE values because the overall structure of these two neural networks is very close. On the other hand, the comparison of the MAPE values of these two methods in each analyte indicated the significant reduction of prediction error in ANN-GA which refers to the high potential of ANN-GA for application in complex processes.

3.3. Optimization by shuffled frog leaping algorithm

SFLA as a new meta-algorithm was applied to find the optimum amounts for the input parameters, that is, pH, time, amount of biosorbent, temperature, and initial dye concentration, based on the outputs of the ANN with the lowest MSE achieved for the predictive values. The SFLA algorithm was coded in the MATLAB R2015 environment. Therefore, the lower and upper limits of the input parameters (as shown in Table 2) are completely intelligent and based on the mechanism of the SFLA algorithm, it is necessary to identify and report the best values. As the results revealed in Table 2 the optimum values obtained by SFLA were compared with the optimum experimental data which shows high accuracy and ability of this method.

3.4. Effect of pH

The impact of the pH in the range of 1–9 was investigated. The results in Fig. 5a shows that the dye removal (%) increased from 1 to 3 and then constantly maximized at the pH range of 3–4. After that, the removal (%) had a decreasing trend. It seems that in the acidic media (low pH) the adsorbent surface would be positively charged which increases the anionic model dyes adsorption on the surface. Also at the basic media (high pH), the surface of the adsorbent gets negatively charged which leads to the reduction of the electrostatic interaction of anionic dyes (eosin blue and aniline blue) on the negative surface of the adsorbent [8].

3.5. Effect of temperature

In general, the adsorption process can be exothermic or endothermic. Therefore, the effect of temperature is really important in adsorption of the analyte on the sorbent [31]. In the endothermic adsorption process, the rise in temperature results in the increases in the dye removal (%) owing to the adsorption capacity enhancement. In the exothermic

Table 2
Comparison of the optimum results obtained by SFLA and the experimental optimum results

	Experimental	SFLA
pH	3–4	3.345874
Temp	25	25
Amount of biosorbent	10	9.99548
Time	5	5.01642
Initial concentration	10–30	10

Table 1
Functional criteria for prediction eosin blue and aniline blue

	ANN-GA			ANN		
	MSE	MAPE (%)	R^2	MSE	MAPE (%)	R^2
Eosin blue	0.665	0.125	0.915	0.695	0.127	0.810
Aniline blue	0.622	0.119	0.914	0.639	0.120	0.808

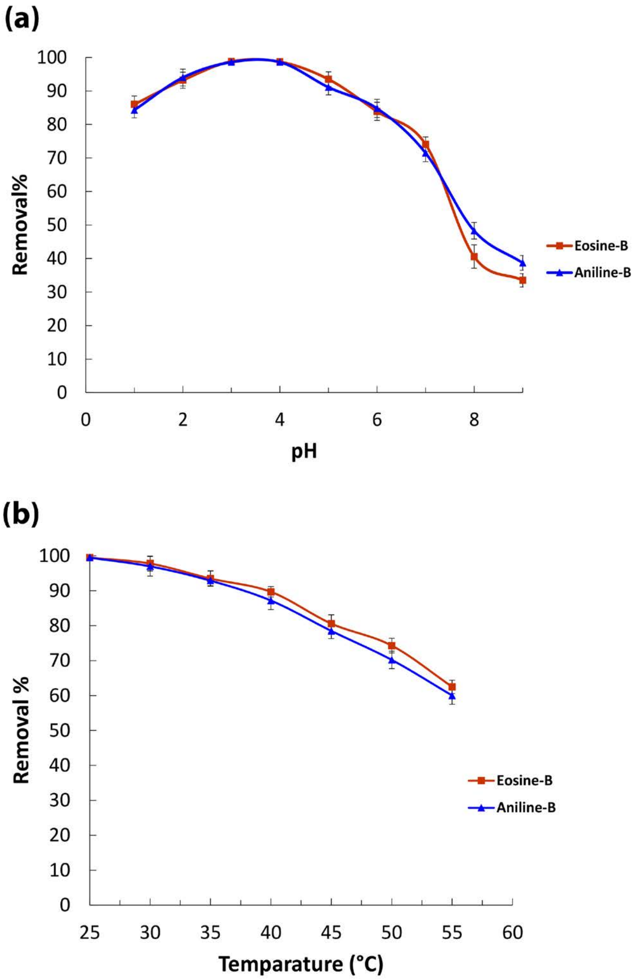

Fig. 5. Effect of parameters of (a) pH (conditions: the amount of biosorbent 50 mg; temperature 25°C; time 15 min; initial dye concentration of 10 mg L^{-1}) and (b) temperature (conditions: pH 3–4; the amount of biosorbent 50 mg; time 15 min; initial dye concentration of 10 mg L^{-1}) on the removal (%) of eosin blue and aniline blue.

adsorption process, the increase in temperature decreases the dye removal (%) due to the decrease in the sportive forces between the active sites of the sorbent and the dye molecules [32]. The effect of the temperature was investigated in the range of 25°C–55°C. As the results indicated in Fig. 5b, by increasing the temperature from 25°C to 55°C the dye removal (%) decreases gradually with a slight slope which refers to the exothermic nature of the adsorption of the anionic dye on the sorbent. Hence, the temperature of 25°C was selected as optimum for further studies.

3.6. Effect of the amount of biosorbent

The vacant binding sites on the bimolecular sorbent surface are the motivating factor in the occupation of these sites by dye molecules. In fact, there is a competition among dye molecules in the solution to settle on the unoccupied sites. Consequently, the more the amount of sorbet is the more the vacant sites are on the sorbent to adsorb the molecules. Furthermore, the contact surface of the adsorbent and the dye molecules would be enhanced [33]. Therefore, the amount of biosorbent in the range of 3–100 mg was considered and the optimum amount of 10 mg was obtained (Fig. 6a).

3.7. Effect of time

Achieving the equilibrium state is essential in all chemical processes which depends on the contact time. Hence, the contact time between the analyte and the adsorbent in the adsorption process definitely influences the dye removal (%) [34]. The contact time in the range of 1–30 min was studied. As time increases from 1 to 5 min, an increasing trend is observed and then, the dye removal (%) is almost constant (Fig. 6b). Consequently, the contact time of 5 min was used.

3.8. Effect of initial dye concentration

The concentration of the interest dye is a dominant factor in the adsorption process, especially on the industrial scale. Obviously, the enhancement in the dye concentration leads to the saturation of active sites of the sorbent [24]. The dye concentration in the range of 10–100 mg L^{-1} was studied. As shown in Fig. 6c, by increasing the concentration from 10 to 30 the dye removal (%) is almost constant and then decreased. The optimum initial concentration in the range of 10–30 mg L^{-1} was chosen.

3.9. Effect of inorganic anion competition

The effect of the exiting anions of sulfate, chloride, and carbonate on adsorption of the target anionic dyes on the surface of curdled milk was investigated. The competition of these anions with anionic dyes for adsorption on the biosorbent with the molar ratios of 0–10 was considered. As the sulfate and chloride anions concentrations increased from 0–7 the removal percent decreased very slightly which is almost neglectable. The increase in the ratios from 7–10, the removal (%) was even slightly higher than that in the absence of chloride or sulfate which might refer to the salting-out effect. The increase in carbonate molar ratio resulted in the reduction of dye removal percent. It seems that carbonate decreased the adsorption of eosin blue and aniline blue on the curdled milk.

3.10. Regeneration of the used biosorbent

The regeneration of the used sorbent is one of the most important points of any kind of sorbent to gain the most profitability. Consequently, the regenerability of the used biosorbent was studied using methanol, ethanol, and acetone. To this aim, the dye-polluted biosorbent and desorption solvent were ultrasonicated for 3 min and the concentration of dyes in the upper phase was determined. The regeneration efficiency was obtained as follows:

$$\text{Regeneration efficiency (\%)} = \text{D.D/A.D}$$

where D.D is the desorbed dye in desorption solvent and A.D is the adsorbed dye on the biosorbent. Ethanol had the

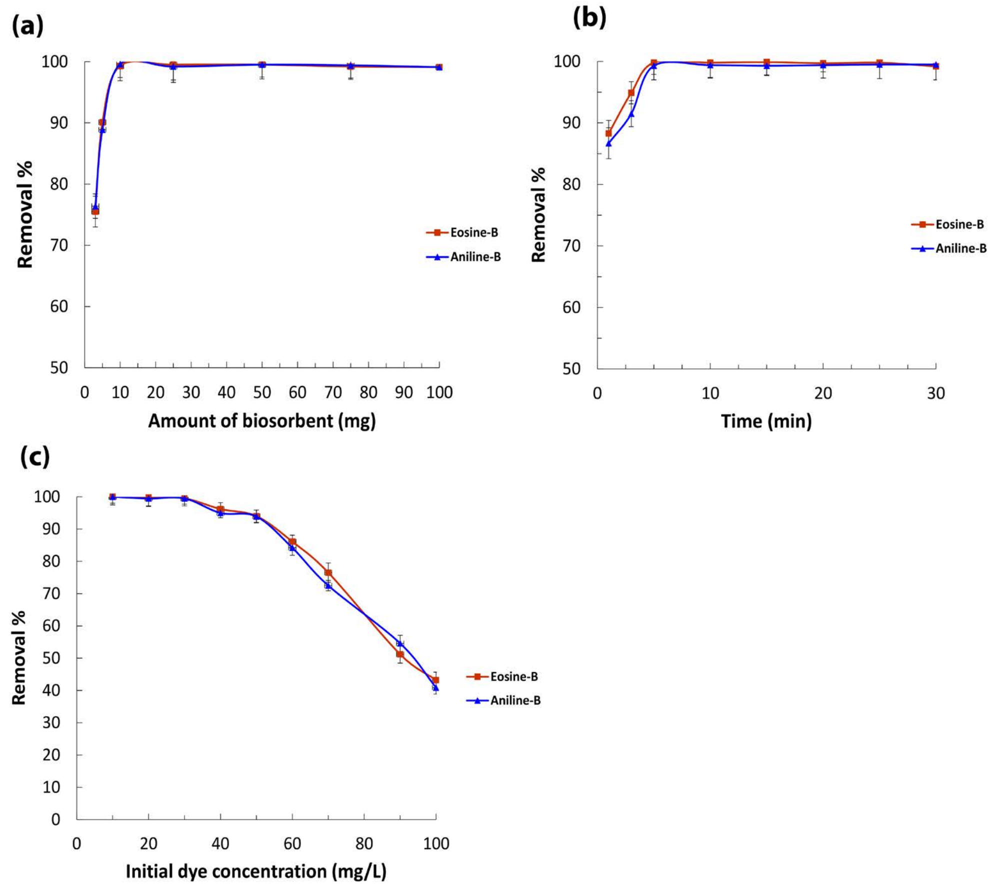

Fig. 6. Effect of parameters of (a) time (conditions: pH 3–4; the amount of biosorbent 10 mg; temperature 25°C; initial dye concentration of 10 mg L^{-1}) and (b) initial dye concentration (conditions: pH 3–4; the amount of biosorbent 10 mg; temperature 25°C; time 5 min) on the removal (%) of eosin blue and aniline blue.

highest regeneration efficiencies of 99.6% and 99.0% for eosin blue and aniline blue, respectively (Fig. 7). Therefore, ethanol was applied as a regeneration solvent of curdled milk in this research study.

In which ethanol had the highest regeneration efficiencies of 99.6% and 99.0% for eosin blue and aniline blue, respectively. Therefore, ethanol was applied as a regeneration solvent of curdled milk in this research study.

3.11. Adsorption isotherms

The adsorptive behaviors of eosin blue and aniline blue onto curdled milk were considered in the batch mode. The equilibrium relationship between the concentration of eosin blue and aniline blue in the sample solution and the adsorbent is depicted by adsorption isotherms to reveal the mechanism of adsorption. Langmuir and Freundlich's isotherms were employed to study the adsorption process. The Langmuir isotherm supposes that adsorption is monolayer and occurs on a homogenous adsorbent surface. The linear Langmuir equation is represented as follows [33,34]:

$$\frac{C_e}{q_e} = \frac{1}{q_m K_L} + \frac{C_e}{q_m} \tag{4}$$

where q_e and q_m (mg g^{-1}) are the amount of adsorbed dye per amount of adsorbent (adsorption capacity) and the maximum adsorption capacity respectively. K_L is the Langmuir constant referring to the affinity of the binding site towards the sorbate (L/mg) q_m and K_L are achieved from the slope and the intercept of the C_e/q_e vs. C_e plot. Another Langmuir parameter is R_L which is called the Langmuir separation factor and is dimensionless. R_L represents the favorability of adsorption of eosin blue and aniline blue onto the curdled milk and is described as Eq. (5) [33]:

$$R_L = \frac{1}{\left(1 + K_L C_0\right)} \tag{5}$$

where C_0 (mg g^{-1}) is the maximum initial dyes concentration. The R_L parameter reveals the unfavorable ($R_L > 1$), linear ($R_L = 1$), favorable ($0 < R_L < 1$), and irreversible ($R_L = 0$) type of the adsorption isotherm. According to the obtained results in Table 3, R_L values for two dyes are $0 < R_L < 1$ which are favorable for adsorption. The Freundlich isotherm is an empirical equation mostly exploits in adsorption processes. The Freundlich isotherm was studied for the present research process. The Freundlich isotherm equation is as follows:

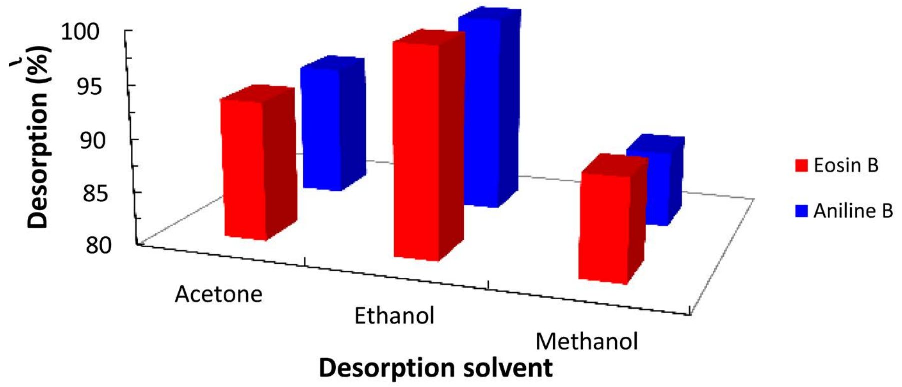

Fig. 7. Effect of desorption solvent type on desorption (%).

Table 3
Isotherm parameters for adsorption of eosin blue and aniline blue onto the curdled milk at the optimum conditions (i.e., pH 3–4; the amount of biosorbent 10 mg; temperature 25°C; time 5 min; initial dye concentration of 20 mg L^{-1})

Dye	Langmuir isotherm				Freundlich isotherm			
	Q_{max} (mg g^{-1})	b (L mg^{-1})	R^2	R_L	K_f	$1/n$	N	R^2
Eosin blue	147.059	0.089	0.9204	0.036	54.137	0.161	6.191	0.8771
Aniline blue	131.579	0.109	0.9519	0.030	51.250	0.158	6.317	0.8734

$$Q_e = K_f C_e^{(1/n)} \tag{6}$$

The linear form of Freundlich isotherm is as follows:

$$\log Q_e = \log K_f + \frac{1}{n}\log C_e \tag{7}$$

In this equation, the K_f is Freundlich constant referring to the adsorbent capacity, and n is the constant indicative of the adsorption intensity. The Langmuir and Freundlich values are all tabulated in Table 3. The Langmuir and Freundlich isotherm plots are illustrated in Figs. 8 and 9. The Freundlich intensity constant for both dyes was as $n > 1$ which reveals the appropriate adsorption of eosin blue and aniline blue even at high ion concentration. Langmuir isotherm plots were obtained by the mean correlation coefficient of 0.9204 and 0.9519 for eosin blue and aniline blue respectively. Also, Langmuir isotherm could satisfactorily describe the adsorption of eosin blue and aniline blue on nano curdled milk.

3.12. Kinetic studies

To assess the kinetic parameters, the four common and standard models of kinetics including pseudo-first-order, the pseudo-second-order, intraparticle diffusion, and Elovich were studied. Lagergren's kinetics equation or pseudo-first-order model is represented as follows:

$$\log\left(q_e - q_t\right) = \log q_e - \frac{K_1}{2.303}t \tag{8}$$

In this equation, K_1 is the rate constant of pseudo-first-order (min^{-1}). The terms q_e (mg g^{-1}) and q_t (mg g^{-1}) are equilibrium adsorption capacity and the adsorption capacity at and at time t (min) respectively. The kinetic parameters were acquired based on the plot of $\log(q_e - q_t)$ vs. t (Figs. 10a and 11a).

The McKay pseudo-second-order model equation is expressed as follows:

$$\frac{t}{q_t} = \frac{1}{K_2 q_e^2} + \frac{t}{q_e} \tag{9}$$

In which K_2 is the rate constant of pseudo-second-order (g mg^{-1} min^{-1}). The plots of t/q_t vs. t were illustrated for aniline blue (Fig. 10b) and eosin blue (Fig. 11b). The theory of intraparticle diffusion was first stated by Weber–Morris model as follows:

$$q_t = k_{\mathrm{dif}} t^{0.5} + C \tag{10}$$

where k_{dif} is the intraparticle diffusion rate constant which indicates the boundary layer thickness. The parameters k_{dif}, C and correlation coefficient are obtained by the slope of the plots of q_t vs. $t^{0.5}$ which is shown in Figs. 10c and 11c for aniline blue and eosin blue respectively. The Elovich kinetic model was also for adsorption of both dyes. The Elovich equation is expressed as follows:

$$q_t = \left(\frac{1}{\beta}\right)\ln\alpha\beta + \left(\frac{1}{\beta}\right)\ln t \tag{11}$$

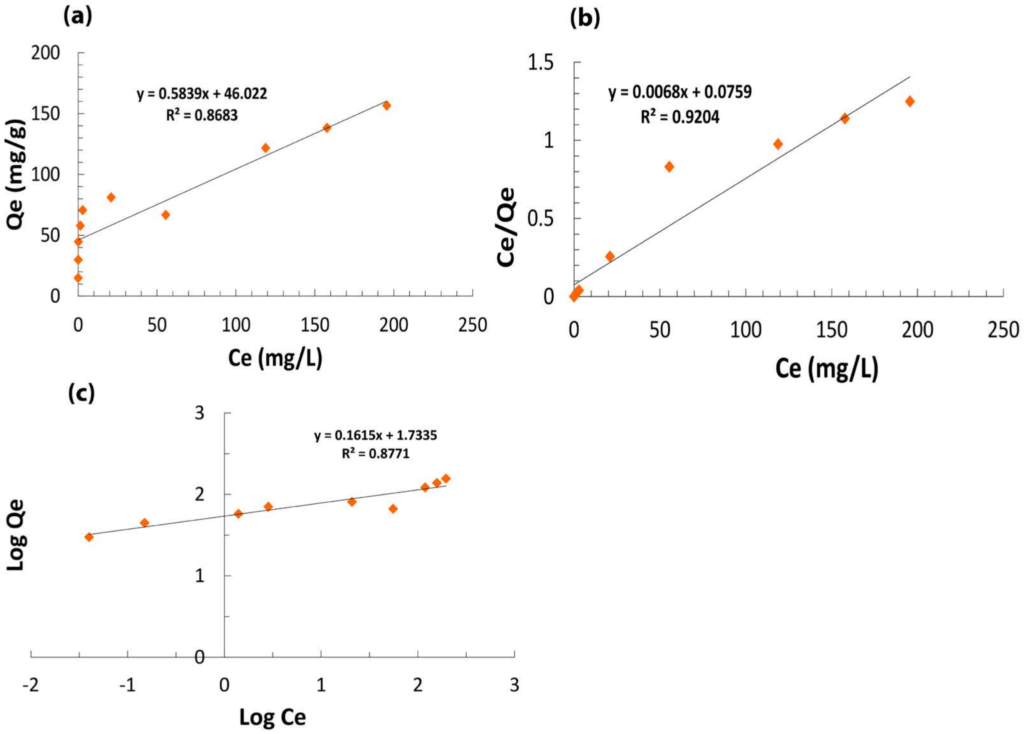

Fig. 8. Adsorption isotherms for eosin blue; Langmuir isotherm plots (a) and (b) and Freundlich isotherm plot (c) obtained at optimum conditions of pH 3–4, amount of biosorbent 10 mg, temperature 25°C, time 5 min.

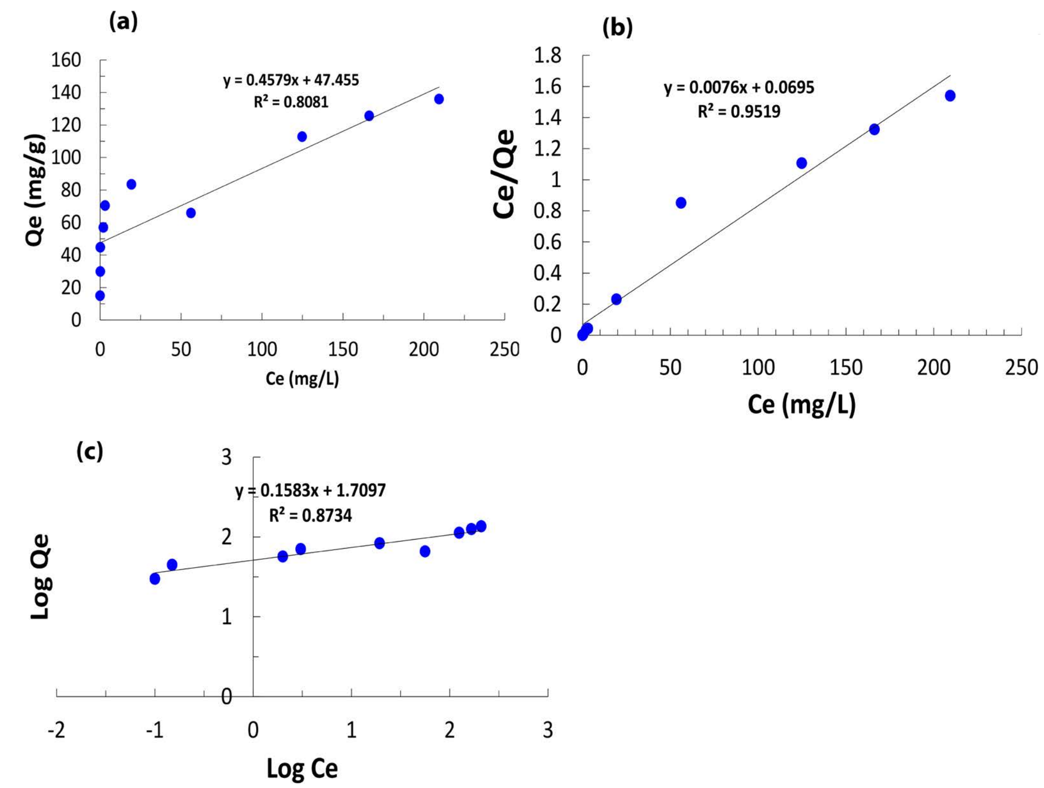

Fig. 9. Adsorption isotherms for aniline blue; Langmuir isotherm plots (a) and (b) and Freundlich isotherm plot (c) obtained at optimum conditions of pH 3–4, amount of biosorbent 10 mg, temperature 25°C, and time 5 min.

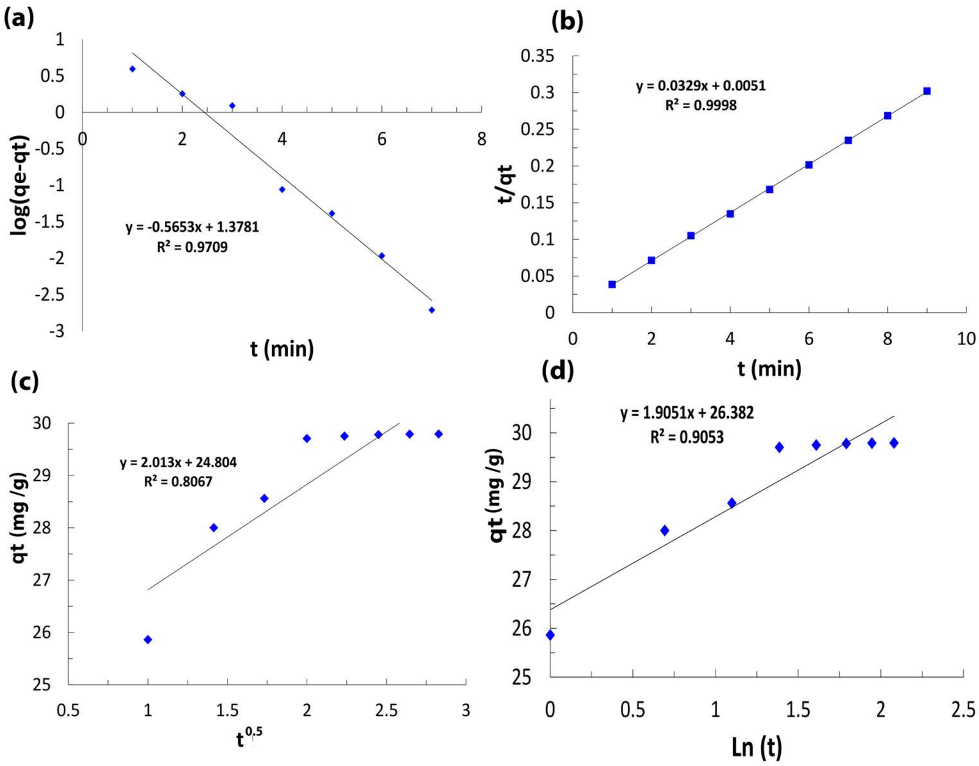

Fig. 10. Kinetic parameters of aniline blue adsorption onto the curdled milk at optimum condition (i.e., pH 3–4; the amount of biosorbent 10 mg; temperature 25°C; initial dye concentration of 20 mg L^{-1}) (a) pseudo-first-order model of Lagergren, (b) pseudo-second-order model, (c) intraparticle diffusion model, and (d) Elovich model.

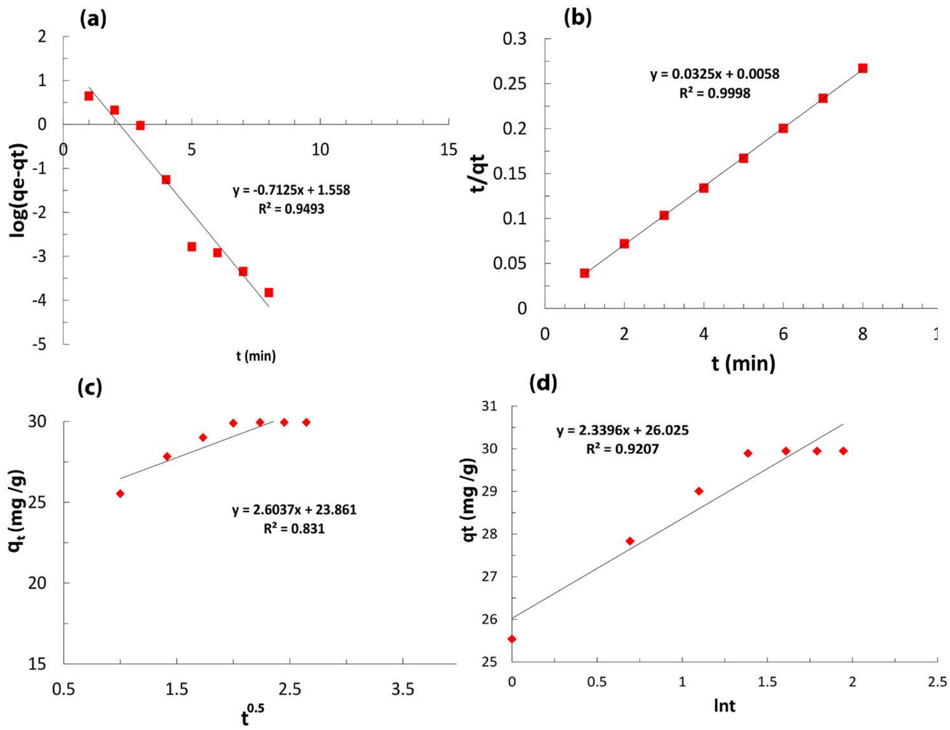

Fig. 11. Kinetic parameters of eosin blue adsorption onto the curdled milk; (a) pseudo-first-order model of Lagergren, (b) pseudo-second-order model, (c) intraparticle diffusion model, and (d) Elovich model.

where α (mg L^{-1} min^{-1}) and β (g mg^{-1}) are the initial rate of adsorption and the extent of surface coverage and activation energy. The results of the kinetic parameters of the four studied models are presented in Table 4a. The correlation coefficient of the pseudo-second-order model is higher and better than the others. Adsorption of aniline blue and eosin blue on to curdled milk follows the pseudo-second-order model.

3.13. Thermodynamic studies

The thermodynamic nature of the proposed adsorption process on the nano biosorbent was explored. The thermodynamic parameters, that is, enthalpy change ($\Delta H°$) and entropy change ($\Delta S°$) and free Gibb's Energy ($\Delta G°$) were achieved based on the following equation [37]:

$$K_c = \frac{q_e}{C_e} \tag{12}$$

where K_c, q_e, and C_e are the equilibrium constant, adsorption at equilibrium (mg g^{-1}), and the equilibrium concentration (mg L^{-1}) respectively. Also, R is the gas constant (8.314 J $mol^{-1}K^{-1}$), and T is the absolute temperature (K). ($\Delta H°$) and ($\Delta S°$) were acquired according to the slopes and the intercepts of the linear plot of the van't Hoff equation (Eq. 14):

$$\ln K_c = \frac{\Delta S°}{R} - \frac{\Delta H°}{RT} \tag{13}$$

$$\Delta G° = \Delta H° - T\Delta S° \tag{14}$$

The plot of lnK_c vs. (1/T) was acquired (Fig. 12). The results are tabulated in Table 4b as follows:

The negative values of $\Delta H°$ confirm the exothermic nature of the adsorption process. Moreover, $\Delta S°$ values of the negative with and for both anionic dyes confirm that the adsorption of aniline blue and eosin blue onto

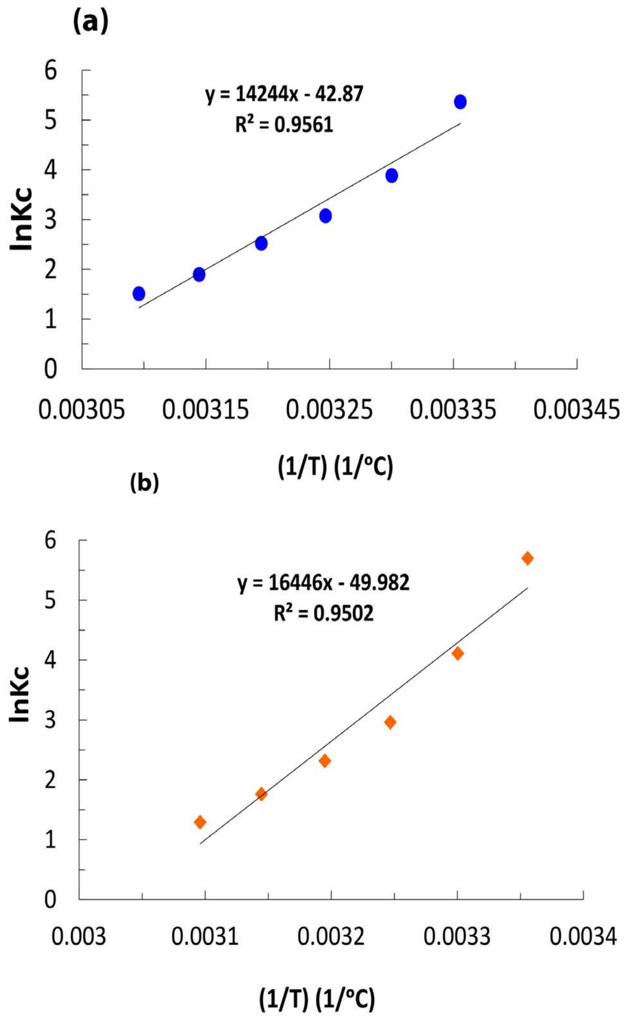

Fig. 12. Thermodynamic study of (a) aniline blue and (b) eosin blue adsorption onto the curdled milk at optimum conditions of pH 3–4, amount of biosorbent 10 mg, time 5 min, and initial dye concentration of 20 mg L^{-1}.

Table 4a

Calculated values of the rate constants of adsorption kinetics and statistical parameters (i.e., pH 3–4, the amount of biosorbent 10 mg; temperature 25°C; initial dye concentration of 20 mg L^{-1})

Kinetic models	Equation	Parameters	Anionic dye	
Pseudo-first-order	$\log(q_e - q_t) = \log q_e - \frac{K_1}{2.303}t$	K_1 (min^{-1})	1.3018	1.6408
		q_e (mg g^{-1})	23.8836	16.9044
		R^2	0.9709	0.9493
Pseudo-second-order	$\frac{t}{q_t} = \frac{1}{K_2 q_e^2} + \frac{t}{q_e}$	K_2 (mg L^{-1} min^{-1})	0.2122	0.1821
		q_e (mg g^{-1})	30.3951	30.7692
		R^2	0.9998	0.9998
Intraparticle diffusion	$q_t = k_{\mathrm{dif}} t^{0.5} + C$	C	24.804	23.861
		K_{diff} (mg L^{-1} $min^{-0.5}$)	2.0130	2.6037
		R^2	0.8067	0.8310
Elovich	$q_t = \left(\frac{1}{\beta}\right)\ln\alpha\beta + \left(\frac{1}{\beta}\right)\ln t$	α (mg L^{-1} min^{-1})	1,968,193	158,526.4
		β (g mg^{-1})	0.5249	0.4274
		R^2	0.9053	0.9207

nano biosorbent is exothermic. The negative values of $\Delta S°$ indicated the decrease in the randomness at solid biosorbent-solute during the exothermic process which led to the regular aggregation and settlement of the dye molecules on the surface of the biosorbent [24]. The negative values of $\Delta G°$ revealed the favorability and spontaneously occurrence of the adsorption process at an optimum temperature of 25°C.

3.14. Adsorption mechanism

The surface characterization of the adsorbent and the chemical structure of the dye is the most important factor to explain the adsorption mechanism. Eosin blue and aniline blue are anionic dyes which efficiently adsorbed onto the biosorbent surface in acidic media (pH in the range of 3–4). Since the structure of curdled milk is polyamide, in acidic media, the $-NH_2$ groups of the biosorbent would change to ammonium groups and efficiently interact with anionic dyes and adsorb them on the surface of curdled milk with high affinity (Fig. 13).

Table 4b
Thermodynamic parameters of the adsorption process of aniline blue and eosin blue onto nano biosorbent at optimum condition (i.e., pH 3–4; the amount of biosorbent 10 mg; time 5 min; initial dye concentration of 20 mg L^{-1})

$$K_c = \frac{q_e}{C_e}$$

$$\ln K_c = \frac{\Delta S°}{R} - \frac{\Delta H°}{RT}$$

$$\Delta G° = \Delta H° - T\Delta S°$$

	$\Delta H°$ (J)	$\Delta S°$ (J)	$\Delta G°$ (J)
Aniline blue	–118.42	–356.42	–12,211.10
Eosin blue	–136.73	–415.55	–12,898.00

3.15. Comparison with other studies

Time and adsorption capacity are two important features that can be compared in dye removal processes. These two parameters can make research study significant among others. Table 5 shows the comparison of removal of eosin blue and aniline blue with curdled milk with other reported studies. As the results show, curdled milk has acceptable maximum adsorption capacities of 147.06 and 131.58 mg g^{-1} for eosin blue and aniline blue respectively which are higher than other reported studies. The proposed biosorbents for removal of eosin blue and aniline blue have the maximum adsorption capacity below 2 (mg g^{-1}). For instance, activated plantain peels carbon and activated carbons both have comparable adsorption capacities with curdled milk. Moreover, significantly higher adsorption capacities of curdled milk for two dyes refer to its nanostructure with higher surface area, polyamide functional groups which can efficiently interact with the target molecules and adsorb them within a shorter time.

4. Conclusions

The novel sustainable protein-based biosorbent, curdled milk, was introduced for removal of eosin blue and aniline

Table 5
Comparison of maximum adsorption capacity of the proposed sorbent with other studies

	Q_{max} (mg g^{-1})		Time (min)		Reference
	Eosin blue	Aniline blue	Eosin blue	Aniline blue	
Sorbent					
HMONs-COOH[a]	51	–	24 h	–	[38]
$Ce_{0.5}Bi_{0.5}CrO_3$ oxide	–	779	–	150	[39]
Microalgae *Chlorella vulgaris*	–	–	–	11 d	[39]
Xanthan-acacia hybrid super-adsorbent	4	–	16 h	–	[40]
ZnO nanoparticles	2.17 g/L	–	70 min	–	[41]
Activated carbon[b]	–	24.54 mg g	–	10 min	[42]
Kaolinites	–	22.6	–	80 min	[43]
Curdled milk	147.1	131.6	5 min	5 min	This study

[a]Carboxyl group functionalized hollow microporous organic nanospheres.
[b]Commercial activated carbon.

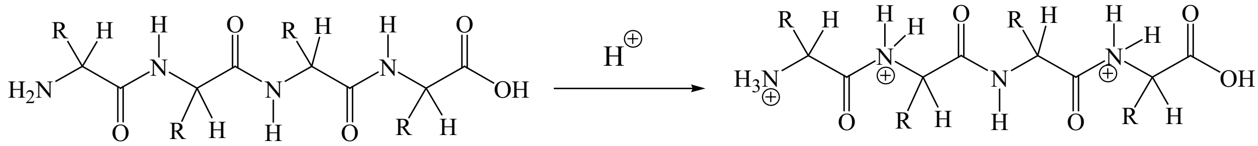

Fig. 13. Structure of curdled milk in acidic media.

blue from aqueous solutions. Hybrid ANN-GA was efficiently utilized for prediction. SFLA was employed successfully for the optimization of the process. At optimal conditions, the removal of 99.5% ± 0.5% and 99.1% ± 0.3% and maximum adsorption capacity of 147.06 and 131.58 mg g^{-1} were achieved for eosin blue and aniline blue respectively which indicated the high capability of the curdled milk. The facile operation, high dye removal percent, highly efficient biosorbent, short extraction solvent are the significant advantages of the proposed method. The introduced sorbent can be effectively applied in a complex mixture of a dye such as textile wastewater which confirms the high potential of the sorbent to be applied in industrial scales.

Acknowledgment

The authors gratefully appreciate the Research Council of the University of Jiroft. This research has been supported by the University of Jiroft under Grant No. 3813–97–6.

References

[1] M. Laissaoui, Y. Elbatal, I. Vioque, G. Manjon, Adsorption of methylene blue on bituminous schists from Tarfaya-Boujdour, Chem. Int., 3 (2017) 343–352.

[2] A. Othmani, A. Kesraoui, M. Seffen, The alternating and direct current effect on the elimination of cationic and anionic dye from aqueous solutions by electrocoagulation and coagulation flocculation, Euro-Medit. J. Environ. Integr., 2 (2017) 6–12.

[3] J. Lin, W. Ye, M.-C. Baltaru, Y.P. Tang, N.J. Bernstein, P. Gao, S. Balta, M. Vlad, A. Volodin, A. Sotto, P. Luis, A.L. Zydney, B. Van der Bruggen, Tight ultrafiltration membranes for enhanced separation of dyes and Na_2SO_4 during textile wastewater treatment, J. Membr. Sci., 514 (2016) 217–228.

[4] I. Chaari, E. Fakhfakh, M. Medhioub, F. Jamoussi, Comparative study on adsorption of cationic and anionic dyes by smectite rich natural clays, J. Mol. Struct., 1179 (2019) 672–677.

[5] S. Khuntia, S.K. Majumder, P. Ghosh, Catalytic ozonation of dye in a microbubble system: hydroxyl radical contribution and effect of salt, J. Environ. Chem. Eng., 4 (2016) 2250–2258.

[6] K. Rahimi, R. Mirzaei, A. Akbari, N. Mirghaffari, Preparation of nanoparticle-modified polymeric adsorbent using wastage fuzzes of mechanized carpet and its application in dye removal from aqueous solution, J. Cleaner Prod., 178 (2018) 373–383.

[7] O. Duman, S. Tunç, T.G. Polat, B.K. Bozoğlan, Synthesis of magnetic oxidized multiwalled carbon nanotube-κ-carrageenan-Fe_3O_4 nanocomposite adsorbent and its application in cationic Methylene Blue dye adsorption, Carbohydr. Polym., 147 (2016) 79–88.

[8] M. Shirani, A. Semnani, H. Haddadi, S. Habibollahi, Optimization of simultaneous removal of methylene blue, crystal violet, and fuchsine from aqueous solutions by magnetic NaY zeolite composite, Water Air Soil Pollut., 225 (2014) 1–15.

[9] S. Hassani, M. Shirani, A. Semnani, M. Hassani, A. Firooz, Removal of Congo red by magnetic nano-alumina using response surface methodology and artificial neural network, Desal. Water Treat., 62 (2017) 241–251.

[10] S. Ghezali, A. Mahdad-Benzerdjeb, M. Ameri, A.Z. Bouyakoub, Adsorption of 2, 4, 6-trichlorophenol on bentonite modified with benzyldimethyltetradecylammonium chloride, Chem. Int., 4 (2018) 24–32.

[11] T.N. Chikwe, R.E. Ekpo, I. Okoye, Competitive adsorption of organic solvents using modified and unmodified calcium bentonite clay mineral, Chem. Int., 4 (2018) 230–239.

[12] S. Mansouri, N. Elhammoudi, S. Aboul-Hrouz, M. Mouiya, L. Makouki, A. Chham, A. Abourriche, H. Hannache, M. Oumam, Elaboration of novel adsorbent from Moroccan oil shale using Plackett–Burman design, Chem. Int., 4 (2018) 7–14.

[13] M.K. Dahri, M.R.R. Kooh, L.B.L. Lim, Water remediation using low cost adsorbent walnut shell for removal of malachite green: equilibrium, kinetics, thermodynamic and regeneration studies, J. Environ. Chem. Eng., 2 (2014) 1434–1444.

[14] E.H. Ezechi, S.R.b.M. Kutty, A. Malakahmad, M.H. Isa, Characterization and optimization of effluent dye removal using a new low cost adsorbent: equilibrium, kinetics and thermodynamic study, Process Saf. Environ. Prot., 98 (2015) 16–32.

[15] H. Daraei, A. Mittal, M. Noorisepehr, J. Mittal, Separation of chromium from water samples using eggshell powder as a low-cost sorbent: kinetic and thermodynamic studies, Desal. Water Treat., 53 (2015) 214–220.

[16] A.L.D. da Rosa, E. Carissimi, G.L. Dotto, H. Sander, L.A. Feris, Biosorption of rhodamine B dye from dyeing stones effluents using the green microalgae *Chlorella pyrenoidosa*, J. Cleaner Prod., 198 (2018) 1302–1310.

[17] F. Hemmati, R. Norouzbeigi, F. Sarbisheh, H. Shayesteh, Malachite green removal using modified sphagnum peat moss as a low-cost biosorbent: kinetic, equilibrium and thermodynamic studies, J. Taiwan Inst. Chem. Eng., 58 (2016) 482–489.

[18] A. Asfaram, M. Ghaedi, S. Hajati, A. Goudarzi, E.A. Dil, Screening and optimization of highly effective ultrasound-assisted simultaneous adsorption of cationic dyes onto Mn-doped Fe_3O_4-nanoparticle-loaded activated carbon, Ultrason. Sonochem., 34 (2017) 1–12.

[19] S. Dashamiri, M. Ghaedi, K. Dashtian, M.R. Rahimi, A. Goudarzi, R. Jannesar, Ultrasonic enhancement of the simultaneous removal of quaternary toxic organic dyes by CuO nanoparticles loaded on activated carbon: central composite design, kinetic and isotherm study, Ultrason. Sonochem., 31 (2016) 546–557.

[20] N. Nedjah, A. Abraham, L.M. Mourelle, Hybrid artificial neural network, Neural Comput. Appl., 16 (2007) 207–208.

[21] H. Liu, F. Yi, H. Yang, Adaptive grouping cloud model shuffled frog leaping algorithm for solving continuous optimization problems, Comput. Intell. Neurosci., 2016 (2016) 1–8.

[22] M.M. Eusuff, K.E. Lansey, Optimization of water distribution network design using the shuffled frog leaping algorithm, J. Water Resour. Plann. Manage., 129 (2003) 210–225.

[23] Y. Xiao, B.H. Li, T. Lin, B. Hou, G. Shi, Y. Li, A Self-adaptive Shuffled Frog Leaping Algorithm for Multivariable PID Controller's Optimal Tuning, L. Zhang, X. Song, Y. Wu, Eds., Theory, Methodology, Tools and Applications for Modeling and Simulation of Complex Systems, 16th Asia Simulation Conference and SCS Autumn Simulation Multi-Conference, AsiaSim/SCS AutumnSim 2016, Beijing, China, October 8–11, 2016, Proceedings, Part I, Springer Singapore, Singapore, 2016, pp. 3–16.

[24] P. Naderi, M. Shirani, A. Semnani, A. Goli, Efficient removal of crystal violet from aqueous solutions with *Centaurea* stem as a novel biodegradable bioadsorbent using response surface methodology and simulated annealing: kinetic, isotherm and thermodynamic studies, Ecotoxicol. Environ. Saf., 163 (2018) 372–381.

[25] J. McCall, Genetic algorithms for modelling and optimisation, J. Comput. Appl. Math., 184 (2005) 205–222.

[26] S. Shakeri, A. Ghassemi, M. Hassani, A. Hajian, Investigation of material removal rate and surface roughness in wire electrical discharge machining process for cementation alloy steel using artificial neural network, Int. J. Adv. Manuf. Technol., 82 (2016) 549–557.

[27] T. Mirzazadeh, F. Mohammadi, M. Soltanieh, E. Joudaki, Optimization of caustic current efficiency in a zero-gap advanced chlor-alkali cell with application of genetic algorithm assisted by artificial neural networks, Chem. Eng. J., 140 (2008) 157–164.

[28] K. Yetilmezsoy, S. Demirel, Artificial neural network (ANN) approach for modeling of Pb(II) adsorption from aqueous solution by Antep pistachio (*Pistacia vera* L.) shells, J. Hazard. Mater., 153 (2008) 1288–1300.

[29] B. Amiri, M. Fathian, A. Maroosi, Application of shuffled frog-leaping algorithm on clustering, Int. J. Adv. Manuf. Technol., 45 (2009) 199–209.

[30] A. Barth, Infrared spectroscopy of proteins, Biochim. Biophys. Acta, Bioenerg., 1767 (2007) 1073–1101.
[31] A.E. Ofomaja, Y.-S. Ho, Equilibrium sorption of anionic dye from aqueous solution by palm kernel fibre as sorbent, Dyes Pigm., 74 (2007) 60–66.
[32] K.-W. Jung, B.H. Choi, M.-J. Hwang, J.-W. Choi, S.-H. Lee, J.-S. Chang, K.-H. Ahn, Adsorptive removal of anionic azo dye from aqueous solution using activated carbon derived from extracted coffee residues, J. Cleaner Prod., 166 (2017) 360–368.
[33] A. Ghazali, M. Shirani, A. Semnani, V. Zare-Shahabadi, M. Nekoeinia, Optimization of crystal violet adsorption onto date palm leaves as a potent biosorbent from aqueous solutions using response surface methodology and ant colony, J. Environ. Chem. Eng., 6 (2018) 3942–3950.
[34] I. Salehi, M. Shirani, A. Semnani, M. Hassani, S. Habibollahi, Comparative study between response surface methodology and artificial neural network for adsorption of Crystal violet on magnetic activated carbon, Arabian J. Sci. Eng., 41 (2016) 2611–2621.
[35] M. Jerold, K. Vasantharaj, D. Joseph, V. Sivasubramanian, Fabrication of hybrid biosorbent nanoscale zero-valent iron-*Sargassum swartzii* biocomposite for the removal of crystal violet from aqueous solution, Int. J. Phytorem., 19 (2017) 214–224.
[36] S.P.D. Monte Blanco, F.B. Scheufele, A.N. Módenes, F.R. Espinoza-Quiñones, P. Marin, A.D. Kroumov, C.E. Borba, Kinetic, equilibrium and thermodynamic phenomenological modeling of reactive dye adsorption onto polymeric adsorbent, Chem. Eng. J., 307 (2017) 466–475.
[37] E.A. Dil, M. Ghaedi, A. Ghaedi, A. Asfaram, M. Jamshidi, M.K. Purkait, Application of artificial neural network and response surface methodology for the removal of crystal violet by zinc oxide nanorods loaded on activate carbon: kinetics and equilibrium study, J. Taiwan Inst. Chem. Eng., 59 (2016) 210–220.
[38] M. Zhou, Z. He, T. Wang, Y. Xu, W. Yu, B. Shi, K. Huang, Carboxyl group functionalized hollow microporous organic nanospheres for efficient catalysis and adsorption, Microporous Mesoporous Mater., 274 (2019) 245–250.
[39] L.A. Awin, M.A. El-Rais, A.M. Etorki, N.A. Mohamed, W.A. Makhlof, Removal of aniline blue from aqueous solutions using Ce1−xBi$x$$CrO_3$ (x = 0, 0.5, 1), Open J. Inorg. Non-met. Mater., 8 (2018) 1–10.
[40] A. Kumar Sharma, Priya, B. Singh Kaith, S. Bajaj, J.K. Bhatia, S. Panchal, N. Sharma, V. Tanwar, Efficient capture of Eosin yellow and Crystal violet with high performance xanthan-acacia hybrid super-adsorbent optimized using response surface methodology, Colloids Surf., B, 175 (2019) 314–323.
[41] R. Mahdavi, S.S. Ashraf Talesh, Enhancement of ultrasound-assisted degradation of Eosin B in the presence of nanoparticles of ZnO as sonocatalyst, Ultrason. Sonochem., 51 (2019) 230–240.
[42] X. You, E. Li, J. Liu, S. Li, Using natural biomacromolecules for adsorptive and enzymatic removal of aniline blue from water, Molecules, 23 (2018) 1606.
[43] H. Koyuncu, A.R. Kul, Removal of aniline from aqueous solution by activated kaolinite: kinetic, equilibrium and thermodynamic studies, Colloids Surf., A, 569 (2019) 59–66.